

This is a repository copy of PLIF flame study on the qualitative and quantitative measurement of OH species for conventional and alternative jet fuels; experimental and theoretical investigations.

White Rose Research Online URL for this paper: https://eprints.whiterose.ac.uk/id/eprint/232781/

Version: Published Version

#### Article:

Saraee, H.S., Hughes, K.J. orcid.org/0000-0002-5273-6998, Shi, S. et al. (1 more author) (2025) PLIF flame study on the qualitative and quantitative measurement of OH species for conventional and alternative jet fuels; experimental and theoretical investigations. Combustion Science and Technology, 197 (11). pp. 2768-2782. ISSN: 0010-2202

https://doi.org/10.1080/00102202.2024.2325511

## Reuse

This article is distributed under the terms of the Creative Commons Attribution-NonCommercial-NoDerivs (CC BY-NC-ND) licence. This licence only allows you to download this work and share it with others as long as you credit the authors, but you can't change the article in any way or use it commercially. More information and the full terms of the licence here: https://creativecommons.org/licenses/

#### Takedown

If you consider content in White Rose Research Online to be in breach of UK law, please notify us by emailing eprints@whiterose.ac.uk including the URL of the record and the reason for the withdrawal request.





# **Combustion Science and Technology**



ISSN: 0010-2202 (Print) 1563-521X (Online) Journal homepage: www.tandfonline.com/journals/gcst20

# PLIF Flame Study on the Qualitative and Quantitative Measurement of OH Species for Conventional and Alternative Jet Fuels; Experimental and Theoretical Investigations

Hossein S. Saraee, Kevin J. Hughes, Si Shi & Mohamed Pourkashanian

**To cite this article:** Hossein S. Saraee, Kevin J. Hughes, Si Shi & Mohamed Pourkashanian (2025) PLIF Flame Study on the Qualitative and Quantitative Measurement of OH Species for Conventional and Alternative Jet Fuels; Experimental and Theoretical Investigations, Combustion Science and Technology, 197:11, 2768-2782, DOI: 10.1080/00102202.2024.2325511

To link to this article: <a href="https://doi.org/10.1080/00102202.2024.2325511">https://doi.org/10.1080/00102202.2024.2325511</a>

9	© 2024 The Author(s). Published with license by Taylor & Francis Group, LLC.
	Published online: 04 Mar 2024.
	Submit your article to this journal 🗗
hil	Article views: 881
Q	View related articles 🗷
CrossMark	View Crossmark data ☑
4	Citing articles: 1 View citing articles 🗷







# PLIF Flame Study on the Qualitative and Quantitative Measurement of OH Species for Conventional and Alternative Jet Fuels; Experimental and Theoretical Investigations

Hossein S. Saraee, Kevin J. Hughes, Si Shi, and Mohamed Pourkashanian

Department of Mechanical Engineering, The University of Sheffield, Sheffield, UK

#### **ABSTRACT**

The hydroxyl molecule is one of the most important intermediate species in the chemistry of combustion processes and plays an important role in the chemical reactions of a hydrocarbon-air flame. However, investigation on a laser-based quantitative measurement of OH in heavy liquid hydrocarbon flames remains very scarce. Thus, in this study, OH radicals were measured qualitatively with the aid of planar laser-induced fluorescence in atmospheric pressure studies of burner stabilized laminar flames of kerosene and alcohol-to-jet (ATJ) fuel. These qualitative profiles were then put on a quantitative basis by analysis of the impact of temperature on the Boltzmann distribution of OH over the ground electronic state rotational energy levels and the use of a simple methane reference flame and its modeling using ANSYS Chemkin-Pro. The quantitative profiles in turn were used to validate the developed chemical kinetic mechanisms of kerosene and ATJ combustion. An experimental apparatus has been developed to investigate the temperature profile and the OH relative amounts of kerosene and ATJ laminar flames in an optimized premixed flat flame burner, under three different air/fuel ratio conditions. Fine wire type thermocouples were applied to provide reliable temperature profiles for the fuel flames. In general, reasonable agreement were observed between the experimental OH results and the simulations for the target fuel flames in the case of kerosene, while a higher peak value of OH was predicted in the ATJ model output compared to the PLIF derived data.

#### ARTICLE HISTORY

Received 28 November 2023 Revised 2 February 2024 Accepted 27 February 2024

#### **KEYWORDS**

Hydroxyl molecule; PLIF; flame; chemical kinetics; quantitative measurement; heavy hydrocarbons

#### Introduction

The desire to better understand combustion and improve its efficiency has led researchers to concentrate on in-depth fundamental investigation of hydrocarbon fuels combustion chemistry, especially in the aviation sector that has an ongoing demand for the foreseeable future for a liquid hydrocarbon fuel (Curran 2019; Dagaut and Cathonnet 2006; Edwards and Maurice 2001; Westbrook and Dryer 1984). One of the areas that requires attention is the analysis of the concentration and distribution of combustion intermediate species, particularly the OH radical, since it plays a key role in the combustion process and can help to gain beneficial

**CONTACT** Hossein S. Saraee Associated hoselfield.ac.uk Department of Mechanical Engineering, The University of Sheffield, Sheffield S3 7RD, UK

underlying knowledge into flame structure of hydrocarbon fuels. Measurement of OH absolute concentration profiles of laminar flames would be of benefit in developing quantitative combustion models that can help researchers to accurately predict the combustion process to aid in the understanding of the performance of practical combustors.

Among the many methods and tools used to conduct research on OH radical measurement, the planar laser-induced fluorescence (PLIF) has attracted much attention.

PLIF has become an important tool for combustion investigations, particularly suitable for fuels flame investigations (Bouvier et al. 2021; Brackmann et al. 2003; Honza et al. 2017; Seitzman and Hanson 1992; Yang et al. 2011). This spectroscopic method is commonly utilized for OH, NO, and other radicals, primarily for qualitative species profile measurement and possibly temperature measurement, and has been proven to be highly sensitive even under extreme conditions (Lackner, Winter, and Agarwal 2013). Commonly, a dye laser is adjusted so that the laser frequency is in resonance with a specific electronic transition in the species being probed. This excites an electron of the chemical species being probed to a higher energy level, which will then emit light (fluorescence) at certain wavelengths as it relaxes back to the ground state. A laser light sheet is generated by suitable optical components and passed through the flame. An image intensifier and CCD camera are used to observe the fluorescence perpendicularly to the light sheet, the intensity of which is proportional to the concentration in the flame. Data is then extracted from the centreline of the flame above the burner surface, which can then be compared to the one-dimensional burner stabilized flame model predictions.

Although a few studies were previously conducted regarding the PLIF qualitative OH measurement of small hydrocarbons such as methane (Cattolica 1982; Chen et al. 2016; Fu et al. 2013; Fuyuto et al. 2010; Hughes, Lightfoot, and Pilling 1992; Schiessl et al. 2004), there is a conspicuous paucity of related empirical investigations on the flames of heavy liquid hydrocarbons such as gasoline, diesel, or jet fuels. This scarcity is more serious in terms of quantitative study of OH species concentration, since there are some challenges such as the lack of knowledge and major uncertainties about the quenching cross sections in these conditions, most previous studies of quenching cross section being focused on quenching by simple colliders (Heard and Henderson 2000; Tamura et al. 1998). In addition, providing a stable flame so that it allows a suitable PLIF recording of OH species at different equivalence ratios of the heavy liquid hydrocarbons flame is very arduous and contributed to a shortage of research in this combustion area.

In this regard, this study aims to determine qualitative measurement of OH radical distribution with the aid of the PLIF technique in two heavy hydrocarbon liquid fuel flames at atmospheric pressure, and then to put these on a quantitative basis by means of analysis of the effect of temperature on the Boltzmann distribution of OH over the ground electronic state rotational energy levels along with comparison to data and simulation concerning a well-characterized flame. Using an optimized burner, a relatively stable laminar flame is provided for the OH PLIF measurement and temperature data of the liquid fuels. A methane/air flame is utilized as the reference fuel to calibrate the results for the target fuels over a range of fuel air ratios. Furthermore, a comparison is made between the PLIF converted quantitative concentration profiles

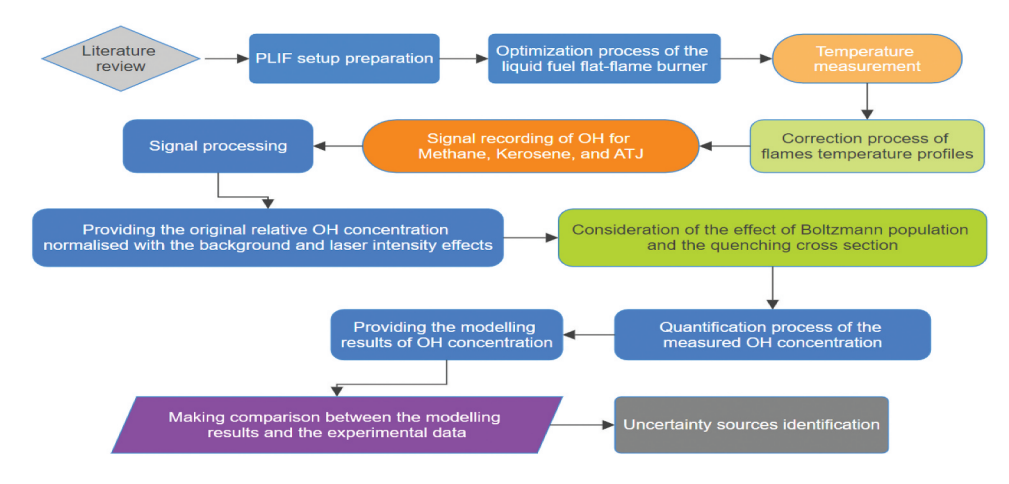


Figure 1. Flowchart diagram of the research working steps.

and the simulated profiles via modeling using ANSYS Chemkin-Pro. A flowchart depicting the overall process is given in Figure 1.

#### Data collection tools and methods

#### Planar laser-induced fluorescence

# LIF working principle

The molecules of a target species such as OH, which exist in a quantum state transit from a ground energy level to a higher level through the absorption of the laser incident light photon at a specified wavelength. In the process of changing the quantum state of the molecule via the light photon, there are three levels of energy for the transition including electronic, vibrational, and rotational, which define the total internal energy of the diatomic molecule. While the electronic energy level is composed of vibrational energy levels (v = 0; 1; ...), the vibrational levels also include rotational energy levels (J = 0) 0; 1; :::). For a thermalized system, the population distribution over the energy states is defined by a Boltzmann distribution that is dependent on the molecule characteristics and the temperature.

A variety of options are available to the excited molecule produced via the absorption of a photon. These consist of emission of a photon of the same wavelength as absorbed, returning the excited species back to its starting point, this is termed "resonance fluorescence." Other options involve emission of a photon at a longer wavelength, "off-resonance fluorescence," which can occur in a variety of ways, such as returning to the ground electronic state but in an excited vibrational energy level, or by processes that involve initial excitation to a higher vibrational energy level in the excited state followed by vibrational energy transfer from this state with subsequent photon emission in returning to the ground electronic state.

In addition to these processes leading to emission of a photon, competing collisional quenching processes can occur that relax the excited molecule to the ground state without any corresponding photon emission. These are not negligible and must be considered for

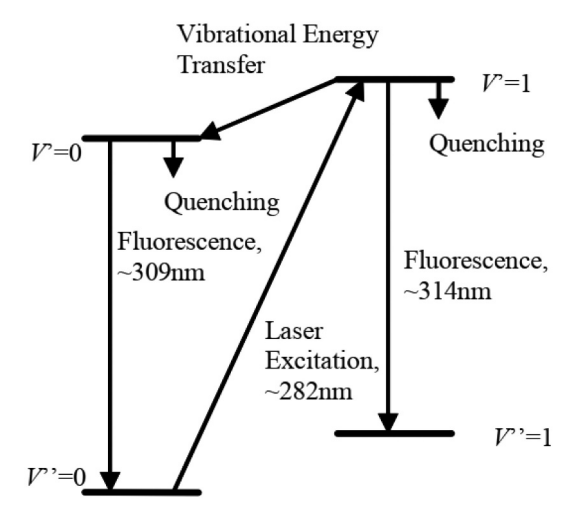


Figure 2. OH energy levels and processes.

the quantification process of the target species concentration. A schematic diagram of OH energy levels and processes including the laser excitation and the various quenching, vibrational energy transfer, and fluorescence processes is given in Figure 2 (Hughes, Pourkashanian, and Wilson 2007).

Transitions are only possible under the selection rules in quantum mechanics so that the orbital angular momentum,  $\Delta L$ , and the total angular momentum,  $\Delta J$  can be equal to -1, 0, and +1, categorized into the branches of P, Q, and R. However, weaker transitions of  $\Delta J = -2$  and +2 can be observed (for the O and S bands), against the selection rules. The OH molecules contain an unpaired electron in a  $2p\pi$ orbital (Maeda, Wall, and Carr 2015), leading to an intrinsic electronic angular momentum of 1/2, and two possible positive or negative spin quantum number for this electron.

#### **PLIF** setup

A Quantel Q-smart 850 Nd:YAG laser was used to create a 1064 nm laser beam, and a second harmonic module (2 ωHG) was applied to double the frequency. A pulsed beam at 10 Hz repetition rate with 5 ns pulse duration at 532 nm in the case of OH PLIF is generated from the Nd:YAG laser and used to pump the Sirah Cobra-Stretch tunable dye laser. The dye laser is then tuned to a wavelength of approximately 566 nm, and a frequency doubling process using a BBO crystal converts these to the required wavelengths of approximately 283 nm for OH. Finally, a laser sheet created by a light sheet optics device is passed through the center of the flame. A LaVision intensified charged couple device (ICCD) camera which was controlled by the DaVis software was utilized to capture the fluorescence signals. The camera was equipped with a specific interference filter in order to allow the fluorescence signal in the 305 to 320 nm range to pass while eliminating the laser scattering.

A schematic setup can be seen in Figure 3, the green lines in the dye laser emulated the laser travel through the cells, and then the generated light sheet is depicted as a transparent cylinder passes through the flame with fluorescence detection by the ICCD camera.

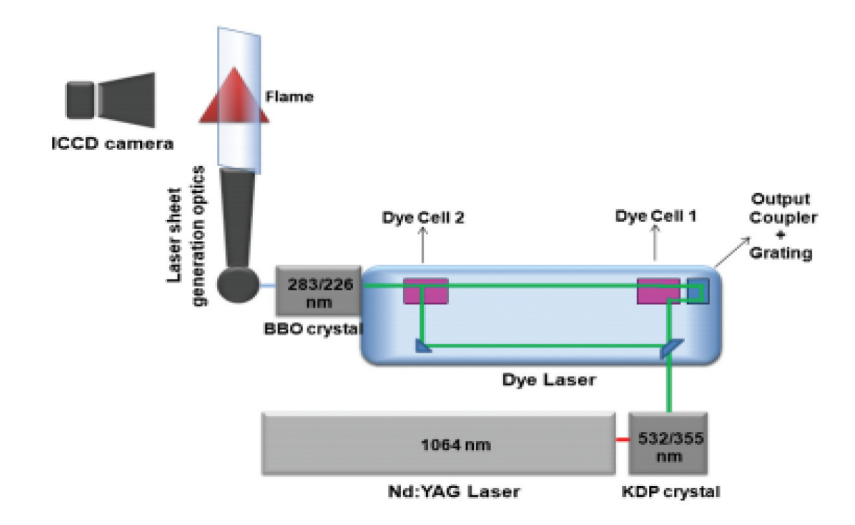


Figure 3. A schematic setup of the laser-induced fluorescence (Catalonotti 2011).

#### **Data collection**

 $A_2\Sigma + \leftarrow X_2\Pi$  (1,0) is the transition from the ground state to the first excited state for OH and Q<sub>1</sub>(6) was preferred as the intended transition to monitor, as it was found from the LIFBASE simulations (Luque and Crosley 1999) to have a high intensity and to be relatively insensitive to the expected temperature range of the flames. The spectrum simulation can be obtained by use of the LIFBASE software to work out precisely which electronic transition is being probed. LIFBASE (LIFBASE 2015) is a free package developed by SRI international, which can calculate the spectroscopic details of the molecules.

Since the laser wavelength practically does not correspond with LIFBASE precisely, calibration of the transition peak was conducted for the accurate positioning of the target signal via scanning a range of wavelengths using the Sirah Control software. To obtain accurate data, the background signal needs to be eliminated because the flame can emit interfering light itself as well as scatter some of the incident laser light. The laser wavelength hence is set to an off-resonance wavelength to measure this background. To ensure the on- and off-resonance laser characteristics are comparable, the off-resonance laser wavelength is set to a value very close to that of the on-resonance wavelength.

To have a high-quality PLIF image, the highest possible intensity of the signal recording is desired that is subject to the safety limitation of the laser power increment and the ICCD camera exposure level. While the target area of the high-intensity species detection is approximately 0-10 mm above the center of the burner plate surface, signals relatively stronger than this desired area of the flame were observed from the edges of the flames because of the direct contact with the open air. Thus, to have the maximum possible intensity at the targeted area and avoid overexposing of the camera, the flame was partially covered by a mask that just allowed observation of the intended area in the middle of the flame and blocked the irrelevant pixels in the edges of the flame.

## **Liquid fuel flat-flame burner**

In this study, an optimized flat-flame burner was utilized to provide a relatively stable premixed laminar flame for the target heavy liquid fuels which have hard-to-manage flames in terms of stability, mainly due to their low volatility and the atomization process. The optimization process was conducted on a burner that was previously designed for liquid hydrocarbon flame studies (Catalonotti 2011) and is illustrated in Figure 5. The fuel flow rate was controlled by a calibrated Brooks Flomega mass-flow controller. Two mass flow controllers were used to control the air, one air stream being used to mix with the liquid fuel and aid the atomization process, the second air stream being subsequently mixed with the atomized liquid fuel/air spray to control the equivalence ratio. The mixture is further mixed by passing through metal shavings, followed by a pipe containing a honeycomb straightener to generate a more uniform laminar flow. Finally, the mixture passes through a holed plate and a uniform flame is formed above the plate surface. An electric heater was applied to heat the mixture through the pipe walls that can promote the spray vaporization and helps to avoid the condensation of the liquid fuels.

At the first step, modification was applied for the nozzle in order to have a more consistent spray, by moving the nozzle toward the top cap and placing it in an optimum position (5–6 mm above the atomizer bar) through a trial and error process.

It was observed that using a soft sintered metal as the diffuser plate cannot effectively tolerate the high flame temperature of the intended heavy liquid hydrocarbon flames. Therefore, solid stainless steel was used to forge the diffuser plate including special patterned meshes with the best possible geometry required for the production of a stable flat-flame. A schematic of the liquid fuel burner can be seen in Figure 4.

#### Temperature measurement

Providing the temperature profile of the target fuels flame is a prerequisite for the calibration of the OH distribution and a necessary input for the simulation of OH profile by the ANSYS Chemkin-Pro burner-stabilized flame simulation tool as the standard software selected for this study. In this regard, temperature measurement was conducted on the flames with the aid of a fine wire 75 µm wire diameter type-R thermocouple with a bead diameter of 187.5 µm at 17 different positions above the burner surface of 0, 0.2, 0.4, 0.6, 0.8, 1, 1.2, 1.4, 1.6, 1.8, 2, 2.5, 3, 4, 5, 7, and 10 mm. To minimize any potential catalytic reactions on the surface of the thermocouple bead at high temperatures, a coating process was conducted on the surface that deposited a thin layer of silica on the wire by means of a micro glass blowing torch and a natural gas/hexamethyldisiloxane flame. The thermocouple signal was collected by an Omega Multiscan 1200 data logger and processed by the software to provide temperature values.

A radiation correction is required to apply on the raw temperature measurements by the thermocouple wire. The following equation introduced by Kaskan (Kaskan 1957) was utilized to be added to the measured temperature (T<sub>raw</sub>) in order to address the radiation losses:

$$\Delta T_{\text{radiation}} = \frac{\left(1.25\varepsilon C_{\text{SB}} T_{\text{raw}}^{4} D^{0.75}\right)}{\lambda (\eta/U)^{0.25}} \tag{1}$$

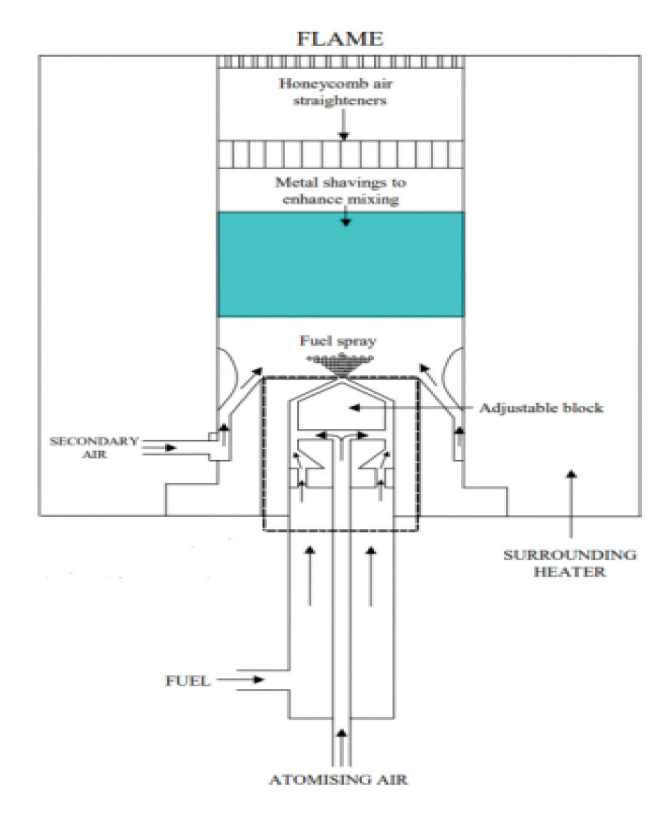


Figure 4. A schematic of the liquid fuel burner (Catalonotti 2011).

Where  $\epsilon$  is the emissivity of the surface of the coated bead (0.2 for silica-coated wire (Kaskan 1957)),  $C_{SB}$  is the Stefan-Boltzmann constant which is  $5.6704 \times 10^{-8}$  J·s<sup>-1</sup>·m<sup>-2</sup>·K<sup>-4</sup>,  $T_{raw}$  is the measured temperature by thermocouples (K), D is the bead diameter (187.5  $\mu$ m),  $\lambda$  is the thermal conductivity of the gas which is approximately  $0.18 \text{ J} \cdot \text{s}^{-1} \cdot \text{m}^{-1} \cdot \text{K}^{1}$  at 1000 K,  $\eta$  is the dynamic viscosity of gases (kg  $\cdot$  m<sup>-1</sup>  $\cdot$  s<sup>-1</sup>) which was extracted from the ANSYS Chemkin-Pro software, and U is the total flow rate  $(kg \cdot m^{-2} \cdot s^{-1})$  that is calculated by a combination of the air and fuel mass flow and the area of the burner plate surface  $(0.000491 \text{ m}^2).$ 

## **Results and discussion**

#### Flame temperature profiles

The results of the raw temperature measurement  $T_m$  and its radiation corrected value  $T_c$  at three equivalence ratios of 0.82, 1, and 1.3 are presented in Tables 1, 2, and Table 3 for methane, kerosene, and ATJ, respectively. The actual total flow rates based on the area of the burner plate surface are given in Table 4.

A similar trend is observed for all the fuel flames, so that the measurement disclosed the highest temperature roughly around 1 mm above the burner surface after a rapid increment from the zero position which has the lowest temperature. Despite having identical preheat temperatures (463 K), at the zero position the flames showed significantly higher, and

Table 1. Temperature profile of methane flames.

Height above	$\varphi =$	0.82	φ=	= 1	$\varphi =$	1.3
the burner/mm	$T_m/K$	$T_c/K$	$T_m/K$	$T_c/K$	$T_m/K$	$T_c/K$
0	1274.7	1316.8	1378.4	1439.6	1524.4	1623.5
0.2	1561.6	1659.9	1601.5	1715.8	1610.4	1735.0
0.4	1655.1	1780.4	1759.0	1928.3	1677.3	1824.9
0.6	1708.8	1852.0	1817.2	2011.1	1715.2	1877.3
0.8	1738.0	1891.6	1824.8	2022.0	1724.1	1889.7
1	1740.8	1895.5	1825.8	2023.5	1728.3	1895.5
1.2	1732.9	1884.6	1810.6	2001.4	1718.6	1882.0
1.4	1725.5	1874.6	1804.9	1993.3	1708.3	1867.8
1.6	1720.0	1867.1	1793.6	1977.1	1700.0	1856.2
1.8	1715.4	1860.8	1789.2	1970.8	1693.0	1846.5
2	1711.5	1855.6	1784.1	1963.6	1687.6	1839.2
2.5	1704.4	1846.1	1778.8	1956.1	1682.2	1831.7
3	1699.4	1839.3	1774.3	1949.7	1673.9	1820.3
4	1692.3	1829.7	1766.6	1938.8	1662.9	1805.3
5	1686.5	1822.0	1760.1	1929.8	1657.3	1797.8
7	1678.4	1811.1	1747.8	1912.5	1651.6	1790.1
10	1666.4	1795.3	1732.2	1890.8	1650.3	1788.4

Table 2. Temperature profile of kerosene flames.

Height above	φ =	0.82	φ =	= 1	φ =	1.3
the burner/mm	$T_m/K$	$T_c/K$	$T_m/K$	$T_c/K$	$T_m/K$	$T_c/K$
0	1139.3	1162.9	1383.7	1439.7	1491.5	1572.3
0.2	1364.8	1414.9	1574.8	1670.9	1615.4	1728.0
0.4	1503.8	1578.9	1714.6	1851.5	1674.4	1805.2
0.6	1612.5	1713.1	1794.8	1960.4	1721.7	1868.6
0.8	1692.5	1815.5	1850.4	2038.5	1770.7	1935.9
1	1776.7	1927.1	1885.0	2088.3	1802.9	1981.0
1.2	1810.2	1972.9	1903.6	2115.4	1811.1	1992.7
1.4	1826.6	1995.5	1897.9	2107.0	1809.1	1989.8
1.6	1824.2	1992.2	1894.9	2102.7	1804.5	1983.3
1.8	1820.2	1986.7	1886.2	2090.0	1798.9	1975.3
2	1814.2	1978.5	1878.7	2079.1	1789.9	1962.7
2.5	1803.5	1963.7	1870.8	2067.7	1777.4	1945.3
3	1794.3	1951.1	1856.8	2047.6	1767.4	1931.4
4	1786.2	1940.1	1859.8	2051.9	1759.1	1919.9
5	1781.8	1934.2	1850.9	2039.3	1751.1	1908.7
7	1773.7	1923.1	1850.4	2038.6	1740.8	1894.7
10	1764.3	1910.4	1844.2	2029.8	1731.0	1881.3

different temperatures which can be attributed to the heat transferred from the flame, relevant to each fuel. The temperature profiles reach to a relatively steady state (after a smooth drop from the peak point). As can be seen in the tables, the values of T<sub>c</sub> are augmented for higher positions above the burner due to the related higher temperatures, mainly as a consequence of the 4th power temperature dependence in the correction equation. As it was expected (Glassman, Yetter, and Glumac 2014), the flames demonstrated the highest temperature at the stoichiometric condition and a lower amount for lean and rich flames. At lean and rich conditions, the generated heat of the combustion process is used to heat the excess air in the lean mixture and the excess fuel in the rich mixture. By comparing the temperature profile of the fuel flames at the same equivalence ratio, it is found that methane has the lower temperature than the heavy liquid fuels due to the lower C/H ratio compared to kerosene and ATJ which have double-bonded carbons with a more

Table 3	Temperature	nrofila	of ATI	flames
Table 5.	remberature	prome	OLALI	names.

Height above	$\varphi =$	0.82	φ =	= 1	$\varphi =$	1.3
the burner/mm	T <sub>m</sub> /K	<i>T<sub>c</sub></i> /K	T <sub>m</sub> /K	$T_c/K$	T <sub>m</sub> /K	<i>T<sub>c</sub></i> /K
0	1148.2	1172.6	1391.4	1448.4	1495.8	1577.7
0.2	1371.3	1422.5	1660.8	1780.0	1629.9	1747.0
0.4	1512.1	1589.1	1770.8	1926.7	1690.7	1827.2
0.6	1639.5	1747.3	1851.7	2039.5	1738.1	1891.2
0.8	1748.2	1889.2	1906.3	2118.2	1778.3	1946.9
1	1820.6	1987.5	1929.3	2152.2	1804.9	1984.2
1.2	1838.0	2011.7	1930.1	2153.4	1826.5	2015.0
1.4	1847.0	2024.3	1923.8	2144.0	1824.7	2012.3
1.6	1845.2	2021.7	1918.1	2135.6	1821.7	2008.0
1.8	1836.8	2010.0	1908.6	2121.6	1812.2	1994.5
2	1832.6	2004.2	1903.2	2113.8	1802.3	1980.6
2.5	1824.6	1993.1	1894.1	2100.4	1794.2	1969.1
3	1815.8	1980.9	1888.0	2091.6	1785.9	1957.5
4	1808.9	1971.3	1879.0	2078.6	1778.8	1947.5
5	1802.2	1962.2	1872.0	2068.4	1773.2	1939.7
7	1791.4	1947.4	1862.8	2055.2	1764.9	1928.2
10	1777.0	1927.8	1849.4	2036.2	1751.7	1910.0

**Table 4.** Flow rates of the fuels  $(kg \cdot m^{-2} \cdot s^{-1})$ .

		Total flow rate	
Fuel	$\varphi = 0.82$	$\varphi = 1$	$\varphi = 1.3$
Methane	0.189	0.157	0.122
Kerosene	0.297	0.239	0.193
ATJ	0.295	0.244	0.192

potential energy release and use less oxygen for the oxidation of H atom leading to the smaller heat capacity and in turn the higher flame temperature (Law 2010).

#### **PLIF OH concentration**

Figure 5 shows the original relative OH concentration normalized with the background and laser intensity effects for the target fuels and methane as the reference fuel and gives an overview for the OH distribution in a 10 mm distance above the burner surface. As can be seen in Figure 5, OH concentration jumped from the lowest amount at zero position to the

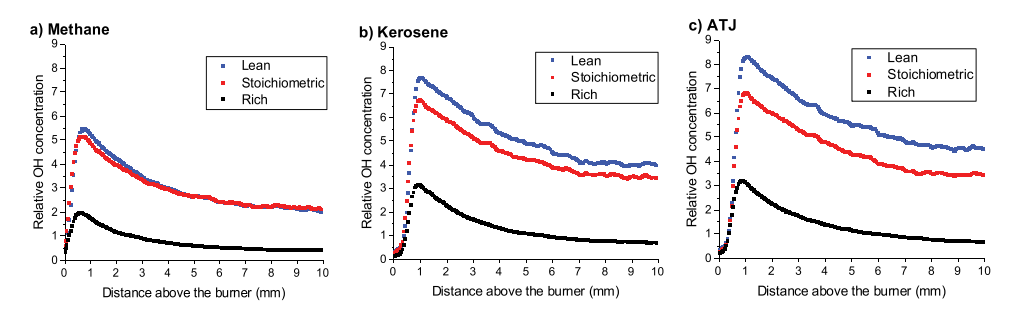


Figure 5. Relative OH concentration of methane (a), kerosene (b), ATJ (c) from Q<sub>1</sub>(6) transition, at lean  $(\phi = 0.82)$ , stoichiometric  $(\phi = 1)$ , and rich  $(\phi = 1.3)$ .

peak value around 1 mm above the burner and then drops slowly. After the generation of OH radical via the reaction of oxygen with the H radicals produced by the H abstraction from the fuels (H +  $O_2 = OH + O$ ), it is dominated by  $H_2/O_2$  reactions until the equilibrium point, that is, the time the OH amount reaches to its peak value and starts to decay.

It is a difficult task subject to many sources of error to directly calibrate the original relative OH concentration. Thus, a calibration strategy can be performed through using a standard reference flame and a simplification process if the signal recording of the fuels flames is conducted under identical conditions including the same detection equipment applied in an identical operational procedure. The relationship of the signal (LIF) to the population of the probed energy level (N) and the total quenching rate (Q) is given by the following expression (Hughes, Pourkashanian, and Wilson 2007):

$$LIF \propto \frac{N}{O}$$
 (2)

Where Q can be calculated by the sum of the quenching cross section ( $\sigma$ ), concentration I, and velocity (V) of the collider species:

$$Q = \sum i\sigma_i C_i V_i \tag{3}$$

And N can be simulated via the LIFBASE software as the Boltzmann population faction (bf) of the probed energy level that is provided as a function from the fitted LIFBASE data illustrated in Figure 6. A rewritten form of the equation 3.1 can be expressed as follows:

$$LIF \propto [OH]bf\sqrt{M}\sqrt{T}\sigma P$$
 (4)

And finally, using the parameters of the standard methane/air flame (LIF<sub>ref</sub>,  $VM_{ref}$ ,  $\sqrt{T_{ref}}$   $\sigma_{ref}$ ) and the fact that the measurements were conducted at the same environment pressure (P) for all fuels, the absolute concentration of the target liquid fuels ([OH<sub>L</sub>]) is achieved as follows:

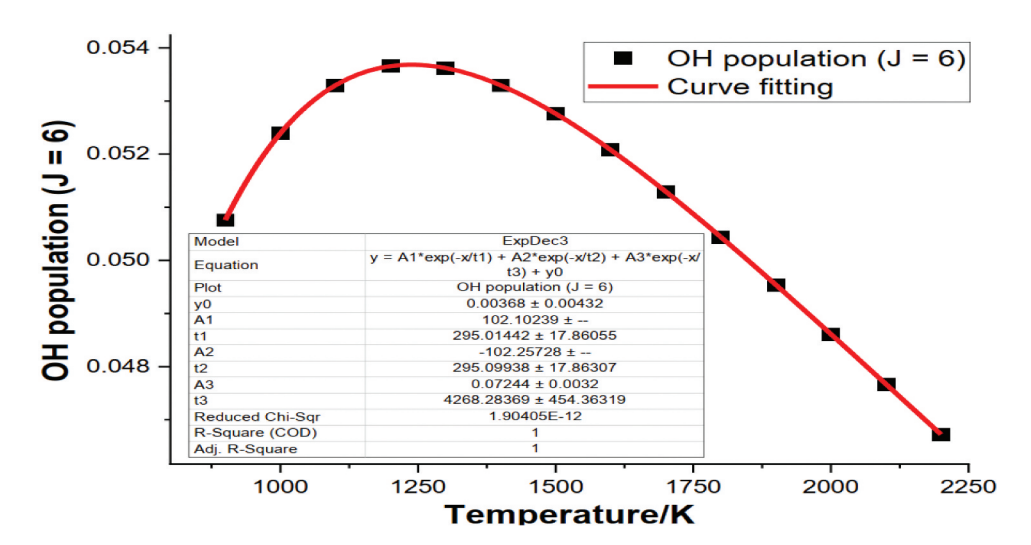


**Figure 6.** Curve fitting plot of the simulated Boltzmann population for OH at J = 6.

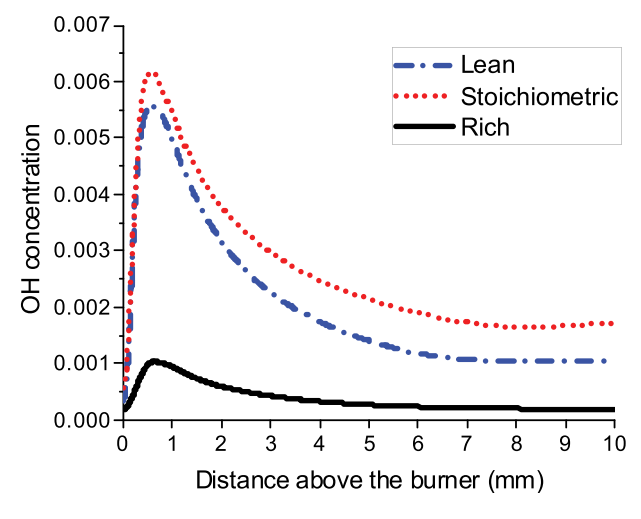
$$[OH]L = \frac{LIF_{L}[OH]_{ref}bf_{ref}\sqrt{M_{ref}\sqrt{T_{ref}}\sigma_{L}}}{LIF_{ref}bf_{L}\sqrt{M_{L}\sqrt{T_{L}}\sigma_{ref}}}$$
(5)

Where the OH mole fraction for methane ( $[OH]_{ref}$ ) is calculated by GRI-Mech 3.0 as the reliable source for an accurate kinetic model, the molecular weight (M) is extracted from ANSYS Chemkin-Pro, the temperature (T) is provided by the thermocouple measurement, and  $\sigma$  is calculated based on Tamura et al.'s work (Tamura et al. 1998) just for the five major colliders of  $N_2$ ,  $O_2$ , CO,  $CO_2$ , and  $H_2O$ , due to the availability of data. The values in the equation 5 can be calculated for a reference point (the maximum or the end point) as the strategy used in this study. By comparing the LIF results of methane with the OH simulation using GRI-Mech 3.0 (figure 7) based on the measured temperature profiles, it was observed that there is a relatively close agreement for the position of the OH maximum point at the three equivalence ratios. While, there is a discrepancy between the model and experimental results for the equilibrium position. Thus, the maximum point seems to be a more reasonable choice for the reference point of the parameter in the equation 5.5. However, the calculations were conducted for both maximum and end points for the fuels and as it was expected, selection of the maximum point showed by far a better result than the end point. Thus, the maximum point results were just included in this study which can be seen in Figure 8.

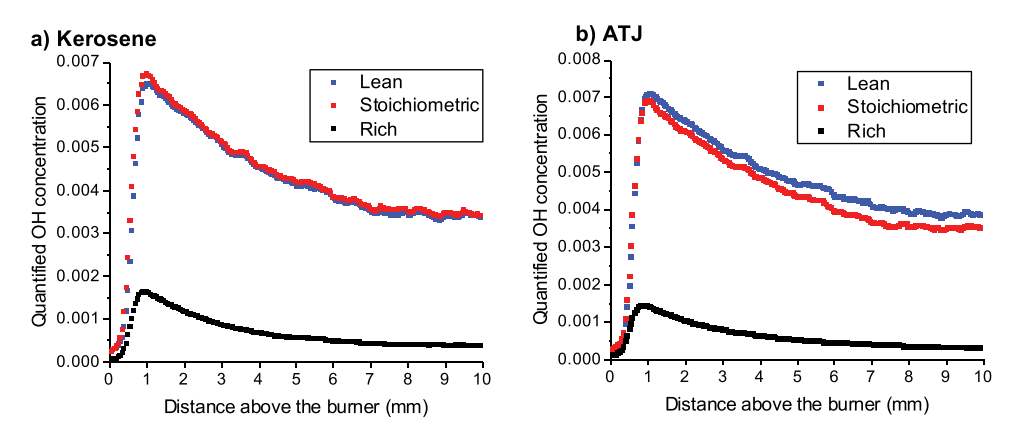
In comparison with the relative OH results of the liquid fuels (Figures 5b,c), the correction process affected the stoichiometric condition more than lean, in terms of OH mole fraction magnitude. This is mainly due to the higher peak value of GRI-Mech 3.0 result (Figure 7) for stoichiometric condition compared to the lean condition, which caused a bigger calibration factor in the equation 5 at the stoichiometric condition of the liquid fuels.

#### Simulated OH concentration

The OH mole fraction of the liquid fuels was simulated by the burner stabilized flame tool in ANSYS Chemkin-Pro through using the previously developed mechanisms of the constructed proposed surrogates for kerosene (Saraee, Hughes, and Pourkashanian 2023b) and ATJ

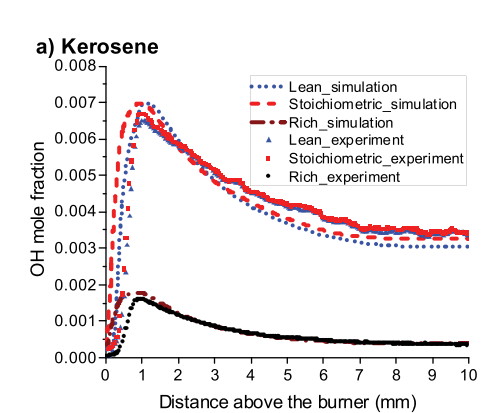


**Figure 7.** Simulated OH concentration using GRIMech 3.0 for the methane reference flames by Chemkin-Pro burner stabilised flame simulation tool, at lean ( $\phi = 0.82$ ), stoichiometric ( $\phi = 1$ ), and rich ( $\phi = 1.3$ ).



**Figure 8.** Quantified OH concentration for kerosene (a) and ATJ (b) at lean ( $\phi = 0.82$ ), stoichiometric ( $\phi = 1$ ), and rich ( $\phi = 1.3$ ).

(Saraee, Hughes, and Pourkashanian 2023a) by the authors of this study. Since the mechanisms could successfully predict the key combustion parameters (ignition delay, laminar flame speed, and species concentration) of the fuels with a close agreement compared to the experimental data in the literature, they were also selected as the appropriate sources for OH prediction in this study. The simulation setup includes the selection of pre-mixed burner tool in the ANSYS Chemkin-Pro software as the suitable reactor for the simulation of the experiment, the preparation of the mechanism, thermodynamics, and transport files as the inputs for the pre-processing step, providing the Reactor physical properties, Grid properties, Species-specific properties, and the required inlet information such as the mass flow rate and the fuel surrogate components. The associated mechanism utilized for the simulation of the kerosene flame is a simplified compact reaction kinetic mechanism developed based on a proposed surrogate consisting of 4 components that are the major components of the real fuel and have the similar property targets to the target fuel. The mechanism applied for the simulation of the ATJ flame (with a chemical formula of C<sub>12.5</sub>H<sub>27.1</sub>) includes isododecane and isocetane sub-mechanisms which are the main components of GEVO ATJ fuel with the properties of Derived Cetane Number = 15.5, Molecular Weight = 176.5 gram/mol, H/C ratio = 2.17, Density = 756 kg/m<sup>-3</sup>, Viscosity = 2.1 cst, Flash point = 48°C, and Smoke Point = 35 mm. As can be seen in Figure 9, in general, there is a relatively close agreement between the simulations and the quantified results for the three equivalence ratios. In terms of the remaining product and the peak value, the burner stabilized flame simulation results of kerosene demonstrate a closer agreement with the quantified experimental results compared to the agreement between the simulation results and experimental data for ATJ fuel. Since the shape of the simulated OH concentration profile is mainly affected by the measured temperature profiles, the simulation results of ATJ fuel showed a higher peak value of OH due to the higher peak temperatures, compared to the respective quantified results. While the only considerable discrepancy for kerosene fuel is the over-prediction of maximum OH at lean condition, the simulation results of ATJ showed an over-prediction for the OH peak values at the three equivalence ratios and for the end points of lean and stoichiometric conditions. Moreover, the model showed a slightly higher OH (after the peak points) at the stoichiometric than the lean compared to the quantified results which obviously demonstrated a higher OH



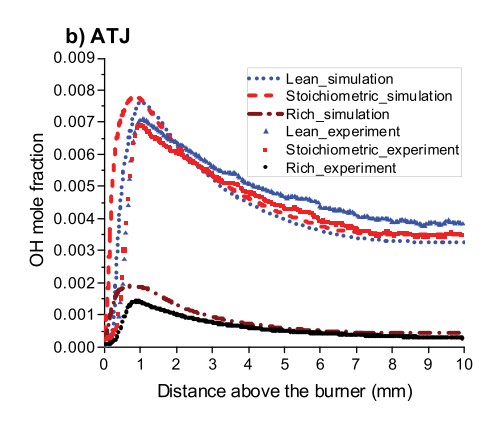


**Figure 9.** Simulated (lines) and quantified (symbols) OH mole fraction for kerosene (a) and ATJ (b) at lean  $(\phi = 0.82)$ , stoichiometric  $(\phi = 1)$ , and rich  $(\phi = 1.3)$ .

for the lean condition than the stoichiometric. This can be related to the ATJ mechanism utilized in this study and/or the uncertainty of the quantification process. Due to the scarcity of the flame investigations on the PLIF quantitative measurement of the liquid fuels key radicals, such as OH, certain levels of errors would be inevitable.

#### **Uncertainty sources identification**

The flat-flame burner utilized in this work provides an open flame with no shrouding gas, while the simulation tool in ANSYS Chemkin-Pro is based on the principle of an adiabatic flame without a mass transfer with the surrounding air. Thus, a discrepancy is expected between the simulation and the experimental results. There are also other sources of uncertainty which can affect the results considerably including; the determination of the distance above the burner surface for the processing of the PLIF images, the radiation correction of the measured temperature, the definition of the zero position for thermocouple measurement, and the relatively high temperature of the first point in the temperature profiles of the stoichiometric and lean conditions (possibly due to the total flow rates). In addition, the process of calculating the quenching cross section is just conducted for the major collider species in the flames. While, it was proved that the hydrocarbon colliders such as methane have a considerable quenching cross-section (Smith and Crosley 1986; Tamura et al. 1998), particularly at the stoichiometric and rich conditions, where there is still a volume of fuel in the mixture. Therefore, a higher correction would be expected for the stoichiometric and rich conditions due to the higher quenching. These are the most significant uncertainty sources that were identified in this study. Addressing all the significant uncertainties would rise another research topic that is out of the scope of this study.

#### **Conclusion**

Planar laser-induced fluorescence is an effective tool to conduct experimental study on the relative measurement of the key species, such as OH radicals, even on the quantitative concentration profile of the species, though it is a challenging task with some sources of uncertainty. Regarding the importance of the hydroxyl molecule in the combustion chemistry of the liquid hydrocarbon fuels and the scarcity of works dedicated to PLIF flame study of heavy liquid fuels, an investigation was conducted on a laser-based quantitative measurement of OH in kerosene and ATJ flames. OH radicals were measured qualitatively and quantitatively with the aid of planar laser-induced fluorescence at the atmospheric pressure condition in an optimized premixed flat flame burner, under three different air/fuel ratio conditions. Coated fine wire type thermocouples were applied to provide reliable temperature profiles for the fuel flames. A methane flame was chosen as the reliable reference fuel and GRI-Mech 3.0 as the reliable methane combustion mechanism was utilized in order to calibrate and quantify the measured relative OH of the liquid fuels. Finally, the converted PLIF OH results were validated using reliable models. In general, a reasonable agreement was observed between the experimental OH results and the simulations for the target fuel flames. In terms of the remaining product and the peak value, the burner stabilized flame simulation results of kerosene demonstrate a closer agreement to the quantified experimental results compared to the agreement between the simulation results and experimental data for ATJ fuel. The simulation results of ATJ fuel showed a higher peak value of OH due to the higher peak temperatures, compared to the respective quantified results. A small over-prediction for the OH peak values was observed for kerosene fuel at just lean condition, and for ATJ at the three equivalence ratios. In spite of the discrepancy and the identified uncertainty sources in this study, the authors believe that this method of using PLIF for the quantitative species concentration profile can be utilized for heavy liquid hydrocarbons.

#### **Disclosure statement**

No potential conflict of interest was reported by the author(s).

#### References

Bouvier, M., G. Cabot, J. Yon, and F. Grisch. 2021. On the use of PIV, LII, PAH-PLIF and OH-PLIF for the study of soot formation and flame structure in a swirl stratified premixed ethylene/air flame. Proc Combust Inst 38 (1):1851–58. doi:10.1016/j.proci.2020.10.002.

Brackmann, C., J. Nygren, X. Bai, Z. Li, H. Bladh, B. Axelsson, I. Denbratt, L. Koopmans, P. E. Bengtsson, and M. Aldén. 2003. Laser-induced fluorescence of formaldehyde in combustion using third harmonic Nd: YAG laser excitation. Spectrochim. Acta A Mol. Biomol. 59 (14):3347-56. doi:10.1016/S1386-1425(03)00163-X.

Catalonotti, E. 2011. Theoretical and experimental investigation of alternative aviation fuels. Doctoral dissertation., University of Leeds.

Cattolica, R. J. 1982. OH radical nonequilibrium in methane/air flat flames. Combust. Flame 44 (1-3):43-59. doi:10.1016/0010-2180(82)90062-1.

Chen, S., T. Su, Z. S. Li, H. C. Bai, B. Yan, and F. R. Yang. 2016. Quantitative measurement of hydroxyl radical (OH) concentration in premixed flat flame by combining laser-induced fluorescence and direct absorption spectroscopy. Chin. Physics B 25 (10):100701. doi:10.1088/1674-1056/ 25/10/100701.

Curran, H. J. 2019. Developing detailed chemical kinetic mechanisms for fuel combustion. Proc Combust Inst 37 (1):57-81. doi:10.1016/j.proci.2018.06.054.



- Dagaut, P., and M. Cathonnet. 2006. The ignition, oxidation, and combustion of kerosene: A review of experimental and kinetic modelling. Prog. Energy Combust. Sci. 32 (1):48-92. doi:10.1016/j.pecs. 2005.10.003.
- Edwards, T., and L. Q. Maurice. 2001. Surrogate mixtures to represent complex aviation and rocket fuels. J. Propuls. Power 17 (2):461-66. doi:10.2514/2.5765.
- Fu, J., C. Tang, W. Jin, L. D. Thi, Z. Huang, and Y. Zhang. 2013. Study on laminar flame speed and flame structure of syngas with varied compositions using OH-PLIF and spectrograph. Int. *J. Hydrogen Energy* 38 (3):1636–43. doi:10.1016/j.ijhydene.2012.11.023.
- Fuyuto, T., H. Kronemayer, B. Lewerich, J. Brübach, T. Fujikawa, K. Akihama, T. Dreier, and C. Schulz. 2010. Temperature and species measurement in a quenching boundary layer on a flat-flame burner. Exp. Fluids 49 (4):783-795. doi:10.1007/s00348-010-0917-x.
- Glassman, I., R. A. Yetter, and N. G. Glumac. 2014. Combustion. Cambridge, Massachusetts: Academic press.
- Heard, D. E., and D. A. Henderson. 2000. Quenching of OH (A 2  $\Sigma$ +, v'= 0) by several collision partners between 200 and 344 K. Cross-section measurements and model comparisons. Phys Chem Chem Phys 2 (1):67-72. doi:10.1039/a908221b.
- Honza, R., C. P. Ding, A. Dreizler, and B. Böhm. 2017. Flame imaging using planar laser induced fluorescence of sulfur dioxide. Appl. Phys. B 123 (9):1-6. doi:10.1007/s00340-017-6823-7.
- Hughes, K. J., P. D. Lightfoot, and M. J. Pilling. 1992. Direct measurements of the peroxy-hydroperoxy radical isomerisation, a key step in hydrocarbon combustion. Chem Phys Lett 191 (6):581-86. doi:10.1016/0009-2614(92)85592-X.
- Hughes, K. J., M. Pourkashanian, and C. W. Wilson. 2007. OH concentration measurements in a jet engine exhaust. Int. J. Energy Clean Environ. 8 (4):305-20. doi:10.1615/InterJEnerCleanEnv.v8.i4.20.
- Kaskan, W. 1957. The dependence of flame temperature on mass burning velocity. Symp. (Int.) Combust. 6 (1):134–143. doi:10.1016/S0082-0784(57)80021-6.
- Lackner, M., F. Winter, and A. K. Agarwal. 2013. Handbook of combustion. Methods 1 (4).
- Law, C. K. 2010. Combustion physics. Cambridge University Press.
- LIFBASE Spectroscopy Tool. 2015. https://www.sri.com/platform/lifbase-spectroscopy-tool/
- Luque, J., and D. R. Crosley. 1999. LIFBASE: Database and spectral simulation program (version 1.5). SRI International Report MP 99-009.
- Maeda, K., M. L. Wall, and L. D. Carr. 2015. Hyperfine structure of the hydroxyl free radical (OH) in electric and magnetic fields. New J. Phys. 17 (4):045014. doi:10.1088/1367-2630/17/4/045014.
- Saraee, H. S., K. J. Hughes, and M. Pourkashanian. 2023a. Development of a surrogate and its comprehensive compact chemical kinetic mechanism for the combustion of ATJ fuel. The European Conference on Fuel and Energy Research and Its Applications, Sheffield, UK, September 4-6.
- Saraee, H. S., K. J. Hughes, and M. Pourkashanian. 2023b. High-fidelity combustion properties modeling of aviation kerosene with the aid of surrogate construction and its simplified chemical kinetics mechanism. In 15th International Conference on Combustion Technologies for a Clean Environment, Lisbon, Portugal, June 25–29.
- Schiessl, R., U. Maas, A. Hoffmann, J. Wolfrum, and C. Schulz. 2004. Method for absolute OH-concentration measurements in premixed flames by LIF and numerical simulations. Appl. Phys. B 79 (6):759-766. doi:10.1007/s00340-004-1576-5.
- Seitzman, J. M., and R. K. Hanson. 1992. Planar fluorescence imaging: Basic concepts for scalar and velocity measurements. Combustings Flow Diagnostics, 137-57.
- Smith, G. P., and D. R. Crosley. 1986. Quenching of OH (A  $2\Sigma$ +, v'= 0) by H2, N2O, and hydrocarbons at elevated temperatures. J. Chem. Phys. 85 (7):3896–3901. doi:10.1063/1.450910.
- Tamura, M., P. A. Berg, J. E. Harrington, J. Luque, J. B. Jeffries, G. P. Smith, and D. R. Crosley. 1998. Collisional quenching of CH (A), OH (A), and NO (A) in low pressure hydrocarbon flames. Combust. Flame 114 (3-4):502-14. doi:10.1016/S0010-2180(97)00324-6.
- Westbrook, C. K., and F. L. Dryer. 1984. Chemical kinetic modeling of hydrocarbon combustion. *Prog. Energy Combust. Sci.* 10 (1):1–57. doi:10.1016/0360-1285(84)90118-7.
- Yang, L., Z. Wang, Y. Zhu, Z. Li, J. Zhou, Z. Huang, and K. Cen. 2011. Premixed jet flame characteristics of syngas using OH planar laser induced fluorescence. Chin. Sci. Bull. 56 (26):2862-2868. doi:10.1007/s11434-011-4630-9.